Volume 1 | Number 1 | Jan 2013 | Pages 1–100

CrystEngComm

www.rsc.org/crystengcomm

ROYAL SOCIETY OF CHEMISTRY

ROYAL SOCIETY OF CHEMISTRY

www.rsc.org/crystengcomm

Journal Name

ARTICLE

Assembly of Binary Ternary and Quaternary Nanorods: From Local to Device Scale Ordering Influenced by Surface Charge

Kevin M. Ryan*,[a] Shalini Singh [a †], Pai Liu [a †] and Ajay Singh[b †]

In this article we outline the assembly of binary, ternary and quaternary nanorods using three separate protocols. The rods are important photoabsorbers CdS, CdSe$_x$S$_{1-x}$, CuIn$_x$Ga$_{1-x}$S, and Cu$_2$ZnSnS$_4$. In the droplet based assembly, we form either 1D rail-tracks or 2D discs of aligned rods depending on the net charge. In the vial based approach, we demonstrate crystallisation of rods into perfectly faceted hexagons. Finally we use electrophoretic deposition to assemble the charged rods directly at the substrate interface to obtain thin-films consisting of 50 or more nanorod layers obtained with complete orientational order.

Introduction

Advances in the colloidal synthesis of compound semiconductor nanocrystals have reached the point where in a single batch synthesis, excellent control of size and shape across the entire particle distribution is routine.[1] Of particular interest are cadmium and copper chalcogenides which have wide band-gaps, excellent absorption coefficients and are of significant application in nanocrystal form for photovoltaics, photocatalysis, thermoelectric conversion and field emission devices.[2–7] The nanorod can be defined as a one-dimensional nanocrystal less than 100 nm in length with aspect ratios that can range from 2-10.[8] The shape anisotropy in rods is of interest for applications that require optimisation of length dependent properties such as total absorption or directional emission and diameter dependent properties such as band-gap.[9,10] Collectively, harnessing the properties of discrete rods for device scale applications requires strategies to assemble them into architectural arrangements- that maximise their packing density and orientational order.[2,11–16] Conceptually, treating the 1D nanocrystals as hard rods, the shape anisotropy is an inherent barrier to the manifestation of long range order over length scales > 1 micron.[2,17,18] The parallels to macroscopic systems such as floating tree logs that organise into raft like arrangements are indeed apparent for some systems e.g. metal nanorods at a liquid air interface.[19] As the rods are further constrained in 2D, the organisation can become more lamellar where side by side packing is further extended. Here, the forces acting on the rods are only external and any organisation is only a function of the system adjusting to allow the most efficient packing. In real systems, various examples of assemblies with longer range order extending over one two and three dimensions have been reported.[10,14,16,20–24]
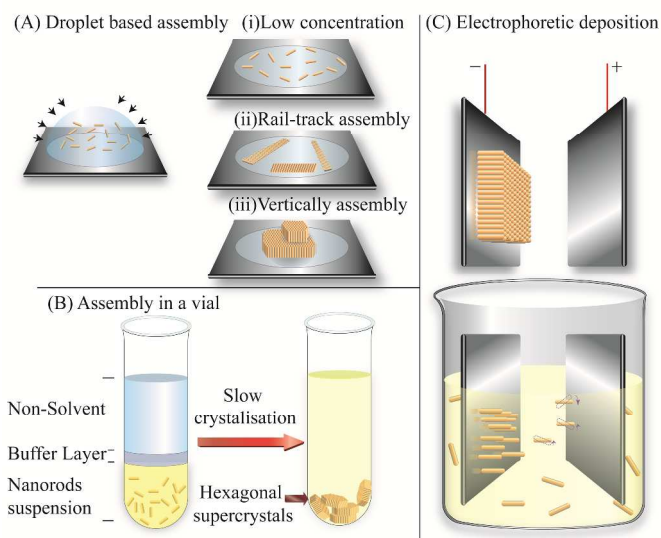
Scheme 1. Three protocols for nanorod assembly: (A) Droplet based assembly, (B) Assembly in a vial and (C) Electrophoretic deposition.

Underlying this is the inaccuracy of ignoring the organic ligand shell on each rod. This critically influences size and shape during synthesis and post synthesis confers dispersibility in non-polar solvents. The ligand shell while increasing the overall spatial volume occupied by the particle also affects the net charge. This is due to either the charge state of the ligand or the extent to which it passivates uncoordinated cationic or

anionic species on the nanocrystal surface.[20,24–27] Although this charge is small (mV), it is significant in terms of the mass of the material in each rod. The other significant feature of colloidal nanorods of compound metal chalcogenides is that they are almost always the wurtzite crystal form with the preference for the axial [001] growth direction giving the desired rod shape.[28–32] This is a non-centrosymmetric lattice that gives rise to a permanent dipole moment (typically of the order of a few hundred Debye) that is also relevant at the length scales in question. Interparticle Columbic interactions therefore become very important in controlling assembly in these systems with or without the influence of external directing agents. Previously we have shown how understanding these factors can allow the assembly from a drying droplet to be tuned from occurrence as 1D rail-tracks or 2D perpendicular assemblies by simply altering the ligand and hence charge.[20,30,33,34] We also demonstrated that the charge allows migration and deposition under an applied field allowing perpendicular assemblies at a surface from solution using electrophoretic deposition.[24,31]

Here, we give a complete description of charge based assembly in colloidal cadmium and copper chalcogenide nanorod systems both in the presence and absence of external directing forces. We show that self-assembly of rods can be directly associated with columbic interactions showing the expected concentration (or interaction length) dependence. Control factors that influence these interactions such as ligand type, solvent dielectric constant and solvent volatility are all shown to influence the final assembly properties. We also consider the important implications of the conditions that assembly occurs, evaporating droplet (Scheme 1A), liquid-liquid interface in a vial (Scheme 1B) and electrophoretic deposition (Scheme 1C). Under close to perfect conditions of slow solvent evaporation, the interactions allow for complete super crystallisation where each rod finds its preferred position on the growing super lattice culminating in a faceted hexagon comprised of close packed and vertically aligned nanorods. For device relevant applications, this can be replicated at a substrate by applying an electric field to the solution resulting in deposition of the charged rods at the opposite electrode. Assembly is demonstrated across a wide range of important colloidal semiconductor rod systems: CdS, $CdSe_xS_{1-x}$, $CuIn_xGa_{1-x}S$ (CIGS), and Cu_2ZnSnS_4 (CZTS). In each system, the control factor is charge and we will further show how the optimal parameter window for assembly can be determined experimentally if physical constants such as dipole moment are not known. The resultant assemblies allow for unprecedented device scale applications where the collective properties of the rods can be harnessed.

Results and discussion

The Building Blocks

Here we look at four colloidal nanorod systems in the binary, ternary and quaternary compositions CdS, $CdSe_xS_{1-x}$, CIGS and CZTS. These are important semiconductors with n-type CdS forming the buffer layer in thin film solar cells and $CdSe_xS_{1-x}$ also n-type with a band gap tunable according to the S/Se composition.[10a] The quaternary p-type semiconductors are important primary absorbers with p-type CIGS showing a typical band gap of 1.85 eV and in thin-film form demonstrating the highest efficiencies.[35–37] CZTS (1.43 eV) is also p-type and benefits from all elements being naturally abundant.[29] Recently, there has been significant interest in
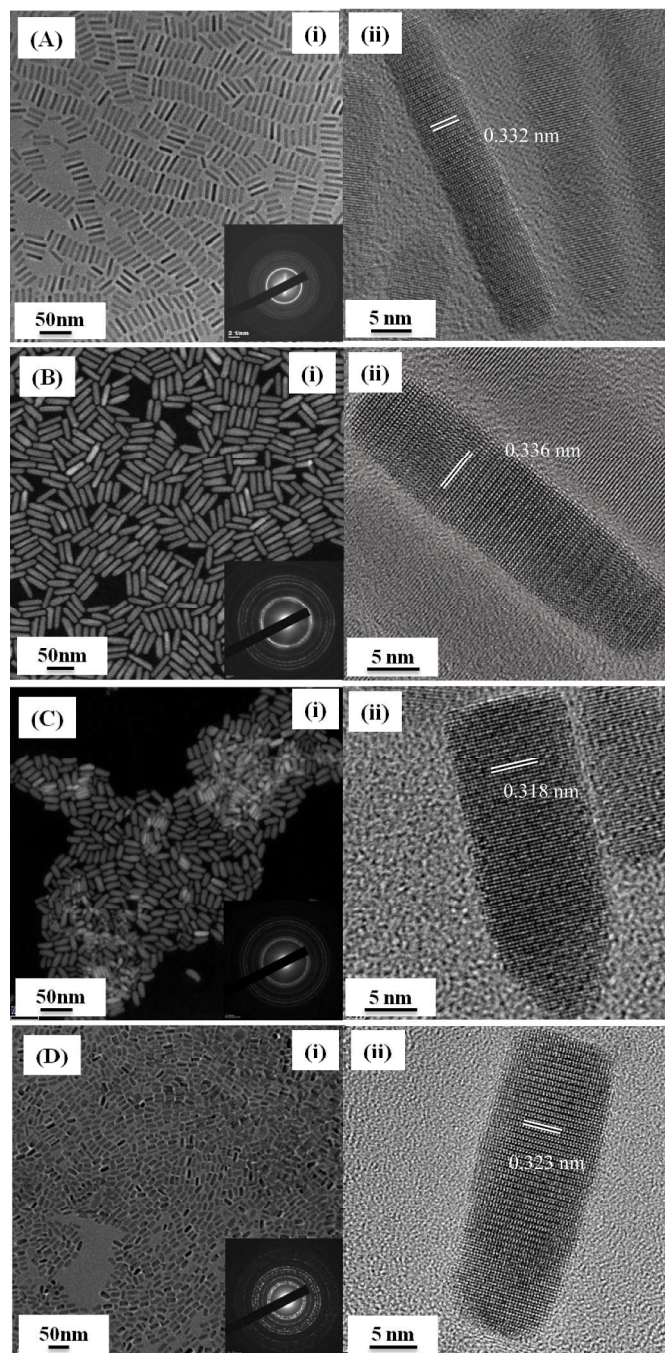
Figure 1. (A) Low Resolution TEM and subsequent HRTEM images of CdS, (B) DF-STEM and subsequent HRTEM of CdSexS1-x,(C) DF-STEM and subsequent HRTEM of CZTS and (D) Low Resolution TEM and subsequent HRTEM images of CIGS nanorods. The insets show the SAED patters of respective nanorods.

developing these layers in nanocrystal/nanorod form due to low energy processing, band gap tunability and their compositional uniformity.[37] Synthetically, the approach to each of these rods is dramatically different with choice of precursors, growth temperature and growth time critical parameters that affect the size, shape and crystal phase of the nanocrystals formed. Generating the rod form requires nucleation and growth in the wurtzite phase with preferential growth along the [001] direction. The choice of ligand combination plays a crucial role

in this process as the different surface energies of the growth facets result in different binding energies thereby allowing preferential growth along the least passivated directions. Although it is very difficult to physically determine actual binding energies of ligands at nanocrystal facets, the effect can be determined by trial and error experimentation. In n-type cadmium chalcogenides, combinations of long chain phosphonic acids and amines are particular effective for fine tuning the chemistry.[30] The requirement of thiols as both a sulphur source and ligand and for the p-type copper chalcogenides complicates these syntheses.[28,29,31] A prerequisite for successful charge based assembly using these rods as building blocks is a narrow distribution in length and diameter across the entire nanorod dispersion. Fig. 1 (A-D) shows low resolution TEM and dark-field scanning transmission electron microscopy (DF-STEM) images for nanorod dispersions and associated HRTEM images for the four nanorod types. CdS nanorods (Figure 1A) have an average length of 35 ± 2 nm and diameter of 7 ± 0.5 nm. $CdSe_xS_{1-x}$ nanorods (Figure 1B) have an average length of 43 ± 2 nm and diameter of 7.5 ± 0.5 nm. CZTS nanorods (Figure 1C) have an average length of 25 ± 3 nm and diameter of 11 ± 2 nm whereas the CIGS nanorods (Figure 1C) have an average length of 27 ± 2 nm and diameter of 7.5 ± 0.5 nm. The HRTEM images show the nanorods are well crystalized and the observed *d*-spacing correspond to (002) planes. The elemental composition of all the different types of nanorods was further confirmed by energy dispersive X-ray (EDX) analysis (Figure S1). The polycrystalline selected-area electron diffraction (SAED) patterns (inset in each) are indexed with rings to (002), (101), and (102), corresponding to the wurtzite phase. The X-ray diffraction spectra (XRD) of CdS, $CdSe_xS_{1-x}$, CZTS and CIGS nanorods Figure S3), demonstrates compositional homogeneity across the nanorod samples. Each XRD pattern consists of a single set of 2θ peaks corresponding to (100), (002), (101), (102), (110), (103) and (112) planes of the hexagonal wurtzite structure.

Understanding the physical properties of each wurtzite nanorod is critical towards developing higher order assembly. Wurtzite rods are known to have a permanent dipole moment due to the non-centrosymmetric lattice that scales with aspect ratio.[29] Additionally our observations have shown that colloidal nanorod systems have a net charge, typically of the order of 5-100 meV, which though small is also significant. This net charge can be estimated by zeta potential studies and interestingly both the magnitude and sign of this charge is affected by the ligand coverage. This combination of low size polydispersity, attractive interactions due to dipole and repulsive interactions due to net charge allow for a rational tool set to control rod organisation based on uniform inter-particle interactions.

Droplet based assembly

The simplest approach to study assembly in a solution of size monodispersed nanorods that are dispersed in an organic solvent is to take a droplet on a TEM grid and allow it to dry. While this is the routine sample preparation for microscopy analysis, there is actually a multitude of factors at play in this system. The drying droplet represents a slowly changing concentration gradient of the rod dispersion in the reducing solvent volume. The droplet however does not shrink uniformly, with successive pinning of the droplet edge, resulting typically in ring patterns as material is deposited due to fluid flow within the droplet. The fundamentals of this
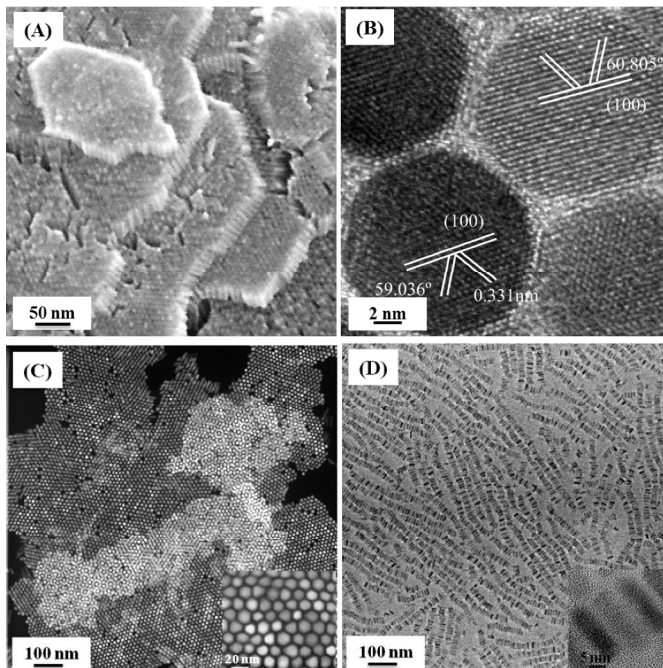
Figure 2. (A) Scanning Electron Microscopy (SEM) images of 2D assembly of CdS nanorods, (B) High resolution TEM images shows the lattice fringes of the drop-cast assembly of CZTS nanorods, (C) DF-STEM of multilayer 2D assembly of $CdSe_xS_{1-x}$ nanorod, with HRDF-STEM in inset, (D) Low resolution TEM of rail track 1D assembly of CdSexS1-x with HR-TEM in inset.

process have been studied for a variety of systems with for example the ring patterns in coffee stains providing the initial conundrum.[34,38] In contrast to a dispersion of coffee particles which will have significant polydispersity, the uniformity of the rod dimensions and hence uniformity of their interparticle interactions creates a more ideal system despite their shape anisotropy. The interactions between the rods can be simplified to columbic forces with repulsion between like charged particles due to net charge offset by dipole-dipole attractions. This interaction has interparticle distance dependence and is therefore greatly affected by the concentration of the particles in solution. Ultimately, the dipole is fixed for a given system and ranges from 150-600 Debye depending on the rod composition and aspect ratio. With a fixed dipole moment, the behaviour of rods in a drying droplet is influenced by a number of factors 1: their net charge which can be approximated by zeta potential, 2: their concentration in solution and 3: dielectric constant of the solvent.[39,40] Modulating the rod charge can be achieved by a facile ligand exchange process with a 40 mV differential between phosphonates/trioctylphosphonic acid capped rods (10 mV) and pyridine capped CdS nanorods (50 mV) sufficient to change the assembly type from 2D perpendicular assemblies to 1D rail-tracks. This is outlined in Figure 2A for phosphonic acid capped CdS rods where the net charge is typically in the range of 10 ± 5 mV. Here the balance of columbic interactions is attractive and at an appropriate concentration, (interparticle distance dependence) rods will aggregate side-by-side in the volume. As the rods orientate in the [001] direction, they attach to each other along the planes perpendicular to this direction (100) and (1-10) planes. This acts as a nucleus for further rod addition with the growing assembly dropping to the surface due to gravity sedimentation.

The resultant assemblies drop down as 2D discs with perfect perpendicular ordering of the rods from edge to centre (Figure 2A). As these discs drop on top of each other, the final sediment consists of multilayers of overlapping 2D sheets of aligned rods. Partial exchange of the rods for pyridine results in rods with a relatively high net charge that are repulsive in solution and therefore the rods have no tendency for aggregation. In a drying droplet, rods where repulsive interactions dominate eventually get pinned at the droplet surface (Scheme 1 A (ii)). Here they are constrained in 2D manifold that is reducing in size resulting in side-by-side dipolar alignment and deposition in 1D rail-tracks (Figure 2B). Further images of 2D and 1D assemblies are shown in the Supporting Information.

  Establishing accurate physical properties of dipole moment and net charge for nanorods is not trivial with the former requiring complex transient dielectric birefringence experiments and the latter typically carried out with zeta potential studies that approximate the rod shape to a sphere. Additionally, the net charge is also affected by the extent of ligand coverage and can be significantly modulated in our observations with repeated anti-solvent precipitations (excess ligand cleaning steps). Adding to this the solvent polarity that screens columbic interactions creates a complex parameter set for predicting the optimum conditions for assembly. A simpler approach is to carry out a study of droplet drying where the only variable is concentration of nanorods in the dispersion. For rods with low net charge (attractive interactions slightly outweigh repulsive), there will exist an optimum concentration for perfect assembly of 2D discs to occur. To further demonstrate the applicability of this approach, we have also taken a system of $CdSe_xS_{1-x}$ alloyed rods. Without knowledge of the dipole moment or net-charge we can tune the assembly from 2D to 1D. The DF-STEM image in Figure 2C shows large scale assemblies obtained by droplet drying when the nanorod concentration in toluene is 9.3×10^{-7} mol/L. Each rod in this layer is perpendicularly aligned from edge to centre. As these discs sediment in the droplet, the deposit on top of each other results in a 3D structure. The resultant Moire Patterns results from a rotational offset between the two hexagonal patterns of each respective disc and the type of pattern ultimately corresponds to the angular offset. Outside of this optimum concentration, nucleation does not occur and the evaporating droplet results in randomly deposited rods.[24,31] $CdSe_xS_{1-x}$ nanorods could also be assembled in the form of 1-D rail-tracks by exchange of the ligands for pyridine similar to CdSe. Interestingly, these rail-tracks could also be achieved via droplet drying of TOPO capped nanorods which have been subjected to extensive cleaning steps (Figure 2D). Here the net charge is sufficient to prevent aggregation in solution and rods get trapped at the interface and deposit as fluid flow moves from the volume of the droplet to the pinned edge during drying. These rail-tracks are typically of the order of 500 nm in length.

Assembly in a Vial

In comparison to a drying droplet, a closed vial of a nanorod dispersion is a simpler system where solvent evaporation, pinning and fluid flow can be discounted. The behaviour of rods under these conditions gives very interesting insights into the processes involved in assembly. For example when a 20 ml vial of CIGS nanorods is allowed to stand for a long period of time > 4 hours, the spontaneous organisation of the rods into ordered 3D assemblies occurs (Figure 3 A-B). The rods align
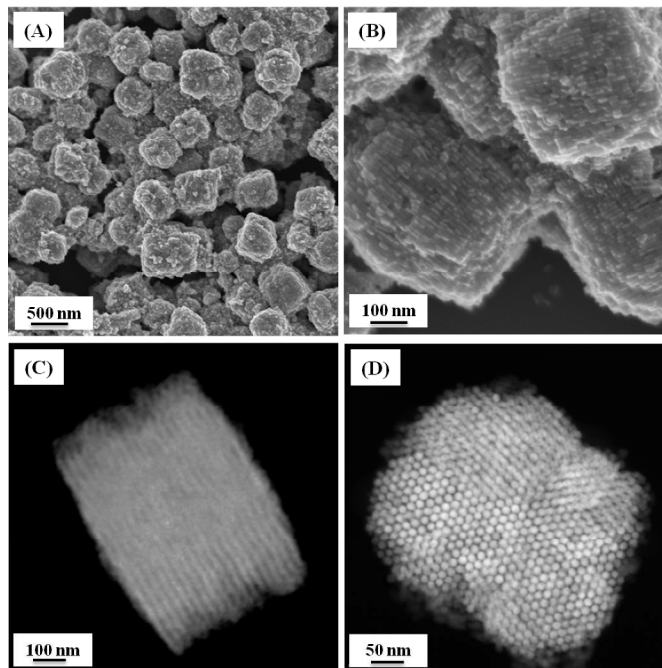
Figure 3. (A) Low resolution TEM images of aligned nanorod clusters of CIGS, (B) Higher resolution image showing aligned rods end to end and side to side within clusters, (C-D) DF-STEM images of side on and end on view of these supercrystals.

perfectly side by side and end to end (Figure 3 C-D) and the number of these clusters and their similar size strongly suggests that this is a crystal growth phenomenon. Further images showing similar clusters with CZTS nanorods are shown in supporting information. At the appropriate supersaturation, many nuclei form and the rods find their preferred place on the growing crystal to maximise their packing efficiency and lower their potential energy. As in all nucleation and growth theory the optimum free energy change occurs as a balance of the dominant attractive (here: dipole-dipole) and repulsive interactions (here: net charge). This is aided by entropic considerations where the system tends to maximum entropy by elimination of solvent volume between adjacent rods. These supercrystals can be disrupted by modulating the rod charge through the introduction of an amine ligand strongly supporting the importance of charge on this process. While these assemblies have perfect side by side and end to end alignment of the rods, the cluster shape is pseudo spherical (Figure 3D). In contrast complete crystallisation that has been observed with 0 D nanocrystals that organise into supercrystals can result in remarkable periodic shapes with perfectly defined facets.[41,42] A feature of this process is that the crystallisation should occur over a long period of time.

  The advantage with 0D nanocrystals is that there is a low rotational barrier to this process.[41] However, the observations of rod assembly both in a droplet and in a vial as outlined demonstrates the interparticle forces involved can overcome anisotropic considerations for nucleation of supercrystals. Achieving long range and defined order in these crystals requires longer growth times.[43] The most effective way to achieve this is by using a three layer oversaturation technique where the solvent (e.g. toluene) is separated from the appropriate non-solvent (methanol) using a buffer layer (isopropanol). The slow diffusion of the non-solvent into the
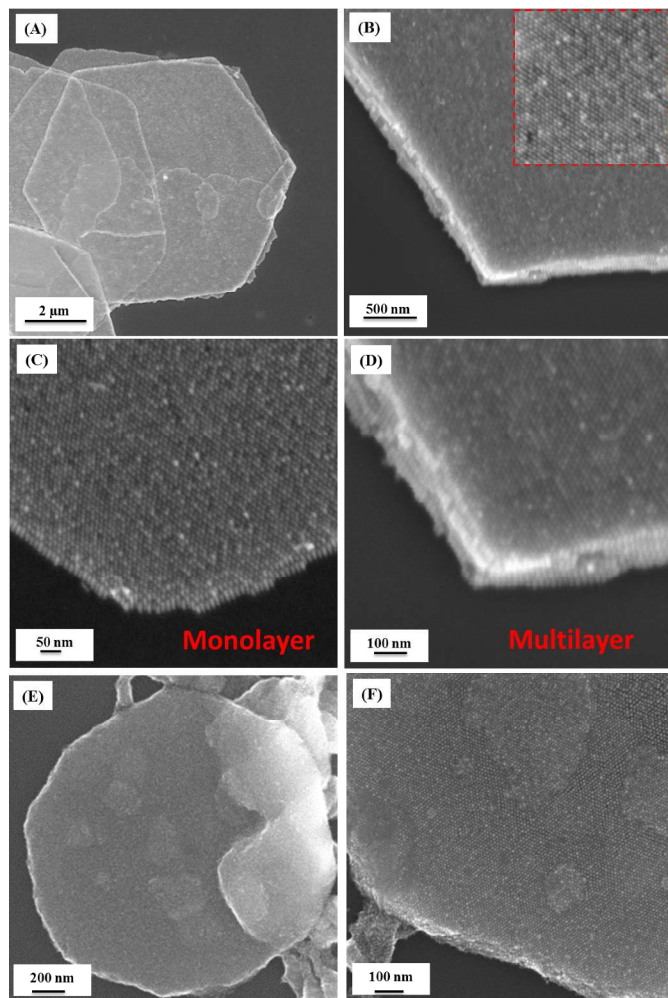
Figure 4. (A) Low Resolution SEM image of perfectly hexagonal faceted discs obtained by slow crystallization of CdS nanorods, (B) Edge view and top view inset showing the extent of faceting and close packing of the rods inset. (C) Monolayer hexagon (D) Multilayer Hexagon, (E-F) Crystallisation with CdSe$_x$S$_{1-x}$.

nanocrystal dispersion allows a very gradual change in particle dispersibility. Allowing this solution to sit for 2-3 weeks in complete isolation (no external perturbation) allows complete crystallisation of the nanorods. In the case of CdS (Figure 4 A-D) and first time reported CdSe$_x$S1-x (Figure 4 E-F), the rods organise into perfectly hexagonal faceted discs with perfect symmetry demonstrating true crystallisation. High resolution SEM images of these faceted hexagonal crystals (Figure 4 B-C) show that they consist of nanorods perpendicularly aligned and close-packed in plane either as a single monolayer or extending over several multilayers. A detailed investigation of the crystallisation process found that the supercrystal grows layer by layer, with the start of a new layer of nanorods occurring only after the completion of underlying layer and this growth is continuous until all nanorods in the solution are adsorbed on the growing supercrystal. This manifests as a discoloration of the nanorod solution from yellow to colorless. The supercrystal growth process is a two-step event (nucleation and growth) expected for crystallisation processes. The nucleation stage leads to the formation of monolayer hexagon (Figure 4 C) and with further growth of these hexagons (growth stage, Figure 4

D) in the c-direction rod by rod (in-plane) and layer by layer (out of plane).

Assembly by Electrophoretic Deposition

The droplet based and vial based assembly protocols allow for fundamental insights into the assembly processes with respect to colloidal nanorods. From an applications perspective, these approaches have some limitations in that they don't allow for control of assembly size or the location where assembly forms. Additionally as any 3D organisation occurs from the random sequential deposition of 2D discs, they are not compatible with real device processing that would require complete control of rod organisation at a substrate interface. Such controlled assembly can be obtained by using external electric fields to push the rods from solution towards a substrate interface that is placed on the appropriate electrode. This can be achieved in the same non-polar solvents (e.g. toluene) that are used for the droplet based and vial based assembly protocols. In non-polar solvents (low dielectric constant), particle migration is field driven, requiring relatively high voltages (200 V). The capacity for ordered assembly in this system is still defined by the physical properties of the nanorods (charge and dipole moment). Under the influence of an electric field the dipole moment causes the rods to align with electrophoretic migration occurring as a function of net nanorod charge to the oppositely charged electrode.[31] A schematic of this assembly set up is outlined in Scheme 1C. Two electrodes of exactly the same dimensions (to prevent dielectrophoresis) are placed 1mm apart in a vial and a potential difference of 200 V typically for 3-10 minutes is applied. The substrate for assembly can be attached to one of the electrodes if non-conductive or form the electrode if suitably conductive. The mobilities of the particles under the applied field are determined by their net charge and their aspect ratio (hydrodynamic radius). For suitable assemblies, rods need to be clean with the minimum of ligand coverage as excess surfactant present will also deposit that greatly affects the uniformity of the deposit particularly between layers.

Concentration of the rods in the dispersion is also important here as it cannot be too high as it will allow for supersaturation and nucleation of assemblies in solution. Figure 5 (A-C) shows SEM cross section images of nanorod assemblies of CdS, CIGS and CdSe$_x$S$_{1-x}$ obtained by EPD. The rods are perfectly aligned with an orientation normal to the substrate in accordance with the direction of the applied field. In addition, the rods show complete side to side order in plane with sequential layers forming directly on top of the underlying deposits for complete space filling. In the p-type rods the incorporation of partial ligand exchange with an amine allows for sufficient net charge on the rods to prevent assembly in solution. The n-type rods (After sequential washing steps) have sufficient electrophoretic mobility for assembly without additional treatment. The results obtained are remarkably consistent across the rod types despite their differences in composition, passivating ligand type and aspect ratio. The optimum conditions for assembly are again best determined experimentally as a function of solution concentrations (below the super-saturation limit) and applied voltage. If the rate of deposition, determined by the applied field, the net charge of the particles and their aspect ratio is too fast, this will lead to disordered deposits.[24,34] The fine balance between obtaining perfect assembly and disordered structures can be understood by again considering the interparticle interactions involved. Under the influence of an applied field, all the rod dipoles will be in the same direction such that these interactions and those of the net charge between the rods will
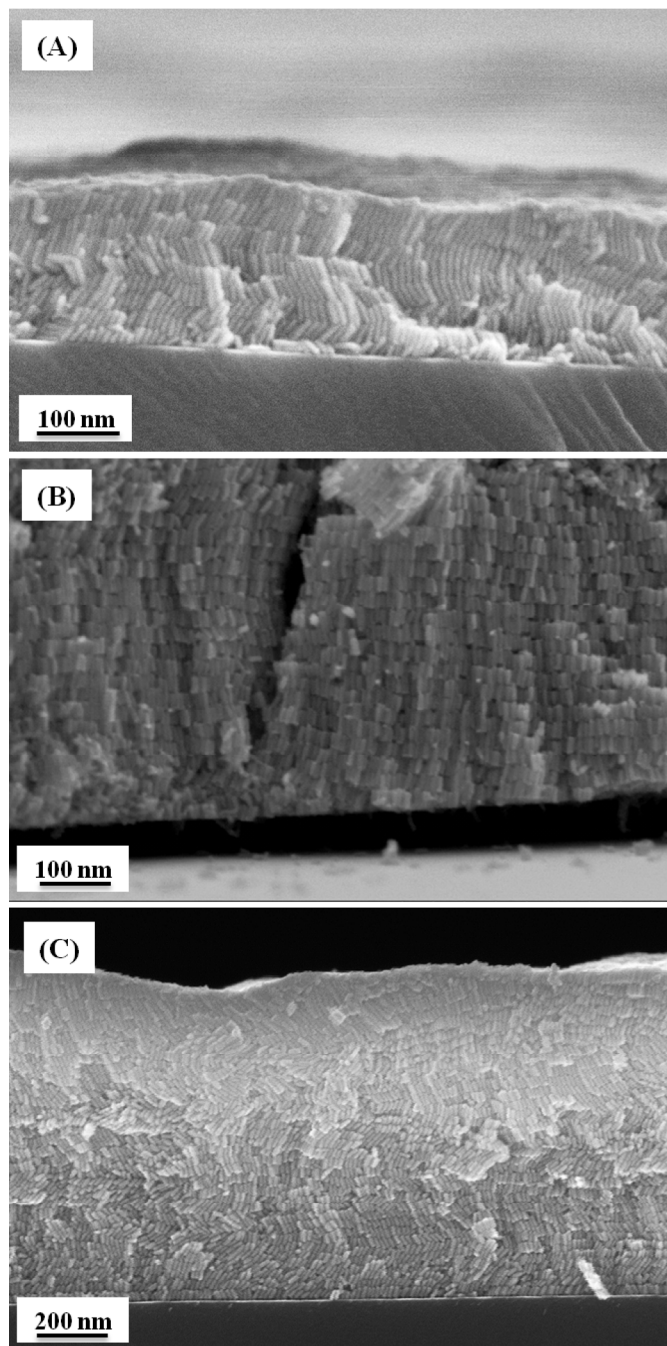
Figure 5. (A-C) SEM cross-section images shows multilayer vertically aligned nanorod assembly over large area obtained by electrophoretic deposition for (A) CdS, (B) CIGS and (C) $CdSe_xS_{1-x}$ nanorods.

be repulsive with the applied field acting opposite to this by pushing the rods together from a 3D volume to the 2D interface. The confluence of these opposing interactions allows incoming rods to find their preferred place on the growing assembly to close pack and align rod by rod and layer by layer. The number of layers obtainable is a function of deposition time allowing for device scale compositions to be obtained where all rods are perfectly aligned and close packed. Figure 5C shows an assembly of $CdSe_xS_{1-x}$ rods extending to a thickness of 1.5 microns from the surface interface. This is the typical thickness of the primary absorber in thin-film solar cells

and was obtained at a solution concentration of 4.6% w/v with an applied voltage of 300V. Considering this totals over 50 layers of aligned rods all close-packed with orientational order, this very effectively demonstrates the capability of EPD to achieve complete control of nanorod assembly where needed.

Standard powder XRD provides a useful tool for non-destructive determination of whether assembly occurs by any of the techniques mentioned. As powder XRD is set up such that in a powder on average sufficient particles will be in the correct orientation to satisfy Bragg's law for each of the repeating planes. For a normal nanocrystal or nanorod dispersion the sample behaves as a powder with no significant difference in relative intensities outside that expected based on structure factor. However when all the rods are aligned in one direction, this complete orientational order has the net effect whereby only the (001), (002) or (004) planes are perpendicular to the beam. Other planes that would only be observed with rods lying on their side are dramatically reduced in intensity. This can be seen from Figure 6 which is obtained from perpendicular assemblies of CdS nanorods where there is a dramatic increase in these peak intensities and almost complete elimination of other reflections. This therefore, provides a highly effective in-line and non-destructive measurement tool to characterise the presence of complete rod assembly within a sample
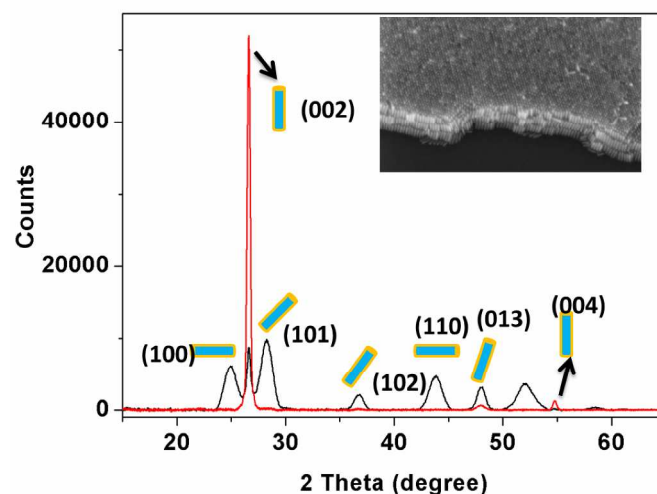
Figure 6. XRD showing increasing in peak intensity of (002) and (004) planes and elimination of other reflections in a perpendicular assembly (red-line) versus random assembly (black line).

Conclusion

Colloidal nanorod assembly is very attractive for applications were the individual and collective rod properties can be harnessed at a device scale. Here we have shown three different assembly protocols, droplet based, vial based and electrophoretic deposition for complete control of nanorod organisation at multiple length scales. The types of assembly obtained range from: 1D rail-tracks; to perfectly faceted hexagonal supercrystals of vertically aligned nanorods; to layered deposits at a substrate extending over 50 aligned and close packed nanorod layers. Importantly, we show that these approaches are generally applicable with assemblies achieved with binary, ternary and quaternary nanorods of both cadmium and copper chalcogenides. The approaches are reproducible despite their different compositions, aspect ratios and ligand chemistries. We have demonstrated the importance of nanorod charge and dipole moment on the interparticle

interactions in each system and hence the assembly process. As these columbic interactions have length dependence, the optimum conditions for assembly can be simplified in each case to a concentration study without exact knowledge of the physical parameters. This bottom up approach to device scale layers of compound semiconductors has many potential advantages over top-down approaches. The colloidal synthesis and deposition protocols are scalable with complete control of stoichiometry in each rod such that in the final layer there is no composition variation. The final devices can retain the discrete rods to harness size and shape dependent properties such as tunable band gap and polarised emission. Alternatively, the rods can be annealed into a bulk thin-film where the uniformity of rod organisation allows greater control of grain boundaries and composition.[44] Ultimately, as the colloidal rods are both synthesised in and processed from solution they allow for low energy and scalable formation of important bulk absorber layers comprised of nanoscale building blocks with complete positional and orientational order.

Experimental

Materials

All reagents were used as received without any further purification. Copper(II) acetylacetonate (Cu(acac)$_2$; >99.99%), Tin(IV) acetate (Sn(OAc)$_4$, >99.99%), Zinc acetate (Zn(OAc)$_2$, >99.99%) Indium(III) acetylacetonate (In(acac)$_3$, 99.99%), Gallium(III) acetylacetonate (Ga(acac)$_3$, 99.99%), Cadmium oxide (>99%) Trioctylphosphine oxide (TOPO, 99%), 1-octadecene (ODE, 90% tech), 1-dodecanethiol (1-DDT, 98%), *tert*-dodecyl mercaptan (t-DDT), Oleylamine (OLA, 70%, technical grade) , was purchased from Sigma Aldrich, Trioctylphosphine (TOP, 90%), Selenium (99.98%), Sulphur (99%), were purchased from Aldrich. n-octadecylphosphonic acid (ODPA), Tetradecylphosphonic acid (TDPA) and n-hexylphosphonic acid (HPA) was obtained from PolyCarbon Industries Inc. (PCI). All solvents were purchased from Sigma Aldrich.

Synthesis of CZTS Nanorods :

Cu(acac)$_2$ (0.261 g, 1 mmol), Zn(OAc)$_2$ (0.091 g, 0.5 mmol), Sn(OAc)$_4$ (0.177 g, 0.5 mmol) and TOPO (1.353 g, 3.5 mmol) were mixed with 10 mL of ODE were added in a three-neck flask and evacuated at room temperature for 30-45 min to remove adventitious water and dissolved oxygen. The reaction mixture was then heated to 250 °C-260 °C under argon flow and a mixture of 0.25 mL of 1-DDT and 1.75 mL of t-DDT was rapidly injected into the system at 150-160°C with continuous stirring. The nanocrystals were allowed to grow for 15-30 minutes to reach the desired size. The reaction was terminated by removal of the heating mantle. After cooling to 80 °C, 2-3 mL of toluene was added to quench the reaction. The nanocrystals were washed 2-3 times in a 1:1 ratio of toluene to ethanol and centrifuged at 3000 rpm for 5 min to yield a brownish centrifuged product. After each centrifugation, the supernatant was removed and the precipitated nanocrystals were redispersed in toluene.

Synthesis of CIGS Nanorods:

For a typical synthesis of CIGS nanocrystals, Cu(acac)$_2$ (0.2618 g, 1 mmol), In(acac)$_3$ (0.3091 g, 0.75 mmol), Ga(acac)$_3$ (0.0918 g, 0.25 mmol), and TOPO (1.3532 g, 3.5 mmol) were mixed with 10 mL of ODE in a three-neck flask. The mixture was evacuated at room temperature for 30 min. The solution was then heated to 250-270 °C in 15-20 min under argon atmosphere. At 155 °C, a mixture of 0.5 mL of 1-DDT and 1.5 mL of t-DDT was injected into the flask which resulted in an immediate colour change from dark green to light yellow. After injection, the reaction was allowed to proceed for 10-15 min with continuous stirring. The heating mantle was

removed and the reaction vessel was allowed to cool to 80 °C. The resulting solution was washed as described for CZTS nanorods.

Synthesis of CdSe$_x$S$_{1-x}$ Nanorods:

Cadmium oxide (0.12g, 1 mmol), TOPO (1.45 g, 3.87 mmol), HPA (0.07g, 4.8 mmol) and ODPA (0.45 g, 1.35 mmol) were mixed in a three-neck flask. Using a heating mantle, the mixture was heated to 120 ºC, evacuated under vacuum for 30 min, and heated to 330 ºC under argon atmosphere to form a completely colourless solution. When the temperature reached 300 ºC, TOP (0.84 g, 2.26 mmol) was injected into the flask. When the temperature reached 330 ºC, 500 µL of TOP-Se-S stock solution was rapidly injected, causing a gradual colour change. After injection, the growth was allowed to continue for 15 min with continuous stirring. Subsequently, the heating mantle was removed and the reaction vessel was allowed to cool to 80 ºC. The resulting solution was washed three times with 1:2 ratio of toluene to IPA for further use.

Synthesis of Cadmium Sulphide (CdS) Nanorods:

Cadmium oxide (0.21 g), TOPO (2.73 g) and ODPA (1.07 g) were weighed out in a 25 mL three-neck flask and heated to 120 ºC under flow or argon. The system was evacuated for one hour to remove any moisture. It was then heated up to 300 ºC and the growth monomer TOP-S was injected in. The nanorods were allowed to grow for 30 min before removal of the heating mantel. When the temperature reached 80 ºC 3 mL of anhydrous toluene was injected in. The nanorods were washed and stored in toluene.

Ligand Exchange of CIGS nanorods:

For ligand exchange, 100 µL of OLA is carefully added to 5 mL of toluene solution of as-synthesized CIGS/CZTS nanorods. With the addition of amine solution an immediate change in the dispersion of the nanorods solution can be visualized. The resulting solution was sonicated for 10 min and then washed with 1:1 ratio of toluene to ethanol and centrifuged at 4000 rpm for 5 min and the supernatant was discarded.

Ligand exchange of nanorods with pyridine:

To prepare pyridine capped nanorods, 1 mL of nanorods solution (0.0013 g mL^{-1}) was dispersed in anhydrous pyridine (5 mL) followed by vortex for 5–10 min and then sonicated for 30 min. The solution was then centrifuged at 13000 rpm for 10 min. The filtrate was discarded and the resulting residue was redispersed in toluene for further study.

Monolayer Assembly of Nanorods:

The self-assembly of nanorods was undertaken by dropcasting the nanorod solution with various concentrations ranging from 10^{-8} to 10^{-2} mol L^{-1} onto carbon supported Cu-TEM grids. The solvent was allowed to evaporate slowly under a constant evaporation rate (in an argon glovebox, with 0% relative humidity).

Multilayer Assembly of Nanorods by Electrophoresis:

For the electrophoresis deposition, the silicon substrate (10 mm x10 mm) was attached on the negative electrode of two parallel gold-coated copper electrodes which were separated at 2 mm apart. A toluene solution of nanorods (10% w/v) was used as electrolyte. The electrodes were completely immersed in a nanorod solution, and a potential of 150-200 V was applied to the electrodes for 3 min using a high voltage power supply unit (TECHNIX SR-5-F-300, S/N: BU08/04971). Voltage was monitored using a Black star 3225 MP millimeter.

Growth of the Superstructure (Hexagon):

The slow crystallization of CdS/ CdSe$_x$S$_{1-x}$ nanorod was carried out through a three-layer oversaturation technique. In a typical experiment, we filled a vial with 3 mL colloidal solution (≈ 10^7 mol L^{-1}) of CdS nanorod in toluene. A buffer layer of 2-propanol (≈ 0.5 mL) was carefully added above the colloidal solution of nanorod. Next, a layer of methanol (3 mL) was added above the buffer layer as shown in Figure 1 b. Extreme care was taken while putting the

methanol layer to make sure the vial was not disturbed. The vial was sealed with paraffin film and left in the glove box undisturbed for approximately two weeks. After 12 days, the decoloration of nanorod solution (yellow) was complete, small sediment was taken out with pipette and dropped on the substrates for SEM, TEM and XRD studies.

Characterization

The nanorods and their assemblies were characterized by transmission electron microscopy (TEM), angular dark-field scanning transmission electron microscopy (DF-STEM) by using a JEOL JEM-2011F operating at accelerating voltage of 200 kV. TEM samples were prepared on 200 mesh carbon-coated copper grids (Ted Pella Inc.). SEM of the assemblies on a Si (111) substrate was performed by a Hitachi SU-70. The samples for X-ray diffraction analysis were prepared by drop-casting the nanorods solution on glass substrates. The analysis was carried out on a PANalytical X0Pert MPD Pro using Cu Kα radiation source (λ = 1.5418 Å) and a 1-D X'celerator strip detector with a 1-D X0Celerator strip detector.

Acknowledgements

Notes and references

[a] Materials and Surface Science Institute and Department of Chemical and Environmental Sciences, University of Limerick, Limerick, Ireland.
[b] The Molecular Foundry, Lawrence Berkeley National Laboratory, 1 Cyclotron Road, Berkeley, California 94720, USA.
† All authors contributed equally.
*Author to whom correspondence should be addressed.

Electronic Supplementary Information (ESI) available: [XRD of all the nanorods, TEM images of assemblies of CZTS nanorods in vials]. See DOI: 10.1039/b000000x/

1. (*a*) R. Krahne, G. Morello, A. Figuerola, C. George, S. Deka, and L. Manna, *Phys. Rep.*, 2011, **501**, 75–221. (*b*) J. Hu, L.-S. Li, W. Yang, L. Manna, L.-W. Wang and A. P. Alivisatos, *Science*, 2001, **292**, 2060; (*c*) Z. A. Peng and X. G. Peng, *J. Am. Chem. Soc.*, 2001, **123**, 183; (*d*) A. Shavel, J. Arbiol and A. Cabot, *J. Am. Chem. Soc.*, 2010, **132**, 4514; (*e*) M. P. Pileni, *J. Phys. Chem. C*, 2007, **111**, 9019 (*f*) A. Shavel, D. Cadavid, M. Ibáñez, A. Carrete and A. Cabot, *J. Am. Chem. Soc.*, 2012, **134**, 1438; (*g*) H. Geaney, C. Dickinson, C. A. Barrett, and K. M. Ryan, *Chem. Mater.*, 2011, **23**, 4838–4843. (*h*) A. Singh, S. Singh, S. Levcenko, T. Unold, F. Laffir and K.M. Ryan, *Angew. Chem., Int. Ed.*, 2013, **52**, 9120; (*i*) C. Coughlan, A. Singh and K. M. Ryan, *Chem. Mater.* 2013, **25**, 653. (*j*) J. Wang, A. Singh, P. Liu, S. Singh, C. Coughlan, Y. Guo and K. M. Ryan, *J. Am. Chem. Soc.*, 2013, **135**, 7835.
2. K. Liu, N. Zhao, and E. Kumacheva, *Chem. Soc. Rev.*, 2011, **40**, 656–71.
3. D. V Talapin, J. Lee, M. V Kovalenko, and E. V Shevchenko, *Chem. Rev.*, 2010, **110**, 389–458.
4. A. E. Saunders, A. Ghezelbash, P. Sood, and B. A. Korgel, *Langmuir*, 2008, **24**, 9043–9.
5. R. E. Bailey and S. Nie, *J. Am. Chem. Soc.*, 2003, **125**, 7100–6.
6. T. Aubert, M. Cirillo, S. Flamee, R. Van Deun, H. Lange, C. Thomsen, and Z. Hens, *Chem. Mater.*, 2013, **25**, 2388–2390.
7. Y. Xie, L. Carbone, C. Nobile, V. Grillo, S. D'Agostino, F. Della Sala, C. Giannini, D. Altamura, C. Oelsner, C. Kryschi, and P. D. Cozzoli, *ACS Nano*, 2013, **7**, 7352–69.
8. X. Peng, L. Manna, W. Yang, J. Wickham, E. Scher, A. Kadavanich, and A. Alivisatos, *Nature*, 2000, **404**, 59–61.
9. A. Singh, H. Geaney, F. Laffir, and K. M. Ryan, *J. Am. Chem. Soc.*, 2012, **134**, 2910–3.
10. D. Kelly, A. Singh, C. A. Barrett, C. O'Sullivan, C. Coughlan, F. R. Laffir, C. O'Dwyer, and K. M. Ryan, *Nanoscale*, 2011, **3**, 4580–3.
11. A. Sanyal, T. Bala, S. Ahmed, A. Singh, A. V. Piterina, T. M. McGloughlin, F. R. Laffir, and K. M. Ryan, *J. Mater. Chem.*, 2009, **19**, 8974.
12. I. Gonzalez-Valls and M. Lira-Cantu, *Energy Environ. Sci.*, 2009, **2**, 19.
13. L. Amirav and A. P. Alivisatos, *J. Phys. Chem. Lett.*, 2010, **1**, 1051–1054.
14. A. Singh, C. Dickinson, and K. M. Ryan, *ACS Nano*, 2012, **6**, 3339–45.
15. J. L. Baker, A. Widmer-Cooper, M. F. Toney, P. L. Geissler, and a P. Alivisatos, *Nano Lett.*, 2010, **10**, 195–201.
16. S. Ahmed and K. M. K. Ryan, *Nano Lett.*, 2007, **7**, 2480–5.
17. M. Zanella, G. Bertoni, I. R. Franchini, R. Brescia, D. Baranov, and L. Manna, *Chem. Commun. (Camb).*, 2011, **47**, 203–5.
18. S. A. Claridge, A. W. Castleman, S. N. Khanna, C. B. Murray, A. Sen, and P. S. Weiss, *ACS Nano*, 2009, **3**, 244–55.
19. X. Ye, C. Zheng, J. Chen, Y. Gao, and C. B. Murray, *Nano Lett.*, 2013, **13**, 765–71.
20. A. Singh, R. D. Gunning, S. Ahmed, C. a. Barrett, N. J. English, J.-A. Garate, and K. M. Ryan, *J. Mater. Chem.*, 2012, **22**, 1562.
21. M. Zanella, R. Gomes, M. Povia, C. Giannini, Y. Zhang, A. Riskin, M. Van Bael, Z. Hens, and L. Manna, *Adv. Mater.*, 2011, **23**, 2205–9.
22. J. B. Rivest, S. L. Swisher, L.-K. Fong, H. Zheng, and a P. Alivisatos, *ACS Nano*, 2011, **5**, 3811–6.
23. X. Lu, Z. Zhuang, Q. Peng, and Y. Li, *CrystEngComm*, 2011, **13**, 4039.
24. A. Singh, N. J. English, and K. M. Ryan, *J. Phys. Chem. B*, 2013, **117**, 1608–15.
25. S. Jia, S. Banerjee, and I. P. Herman, *J. Phys. Chem. C*, 2008, **112**, 162–171.
26. Y. Min, M. Akbulut, K. Kristiansen, Y. Golan, and J. Israelachvili, *Nat. Mater.*, 2008, **7**, 527–38.
27. A. V Titov and P. Král, *Nano Lett.*, 2008, **8**, 3605–12.
28. C. Coughlan, A. Singh, and K. M. Ryan, *Chem. Mater.*, 2013, **25**, 130227065629002.
29. A. Singh, H. Geaney, F. Laffir, and K. M. Ryan, 2–3.
30. S. Singh, A. Singh, K. Palaniappan, and K. M. Ryan, *Chem. Commun. (Camb).*, 2013, **49**, 10293–5.
31. A. Singh, C. Coughlan, F. Laffir, and K. M. Ryan, *ACS Nano*, 2012, **6**, 6977–83.
32. Y.-H. A. Wang, X. Zhang, N. Bao, B. Lin, and A. Gupta, *J. Am. Chem. Soc.*, 2011, **133**, 11072–5.
33. N. Zhao, K. Liu, J. Greener, Z. Nie, and E. Kumacheva, *Nano Lett.*, 2009, **9**, 3077–81.
34. A. Singh, R. D. Gunning, A. Sanyal, and K. M. Ryan, *Chem. Commun. (Camb).*, 2010, **46**, 7193–5.

35. Q. Guo, G. M. Ford, H. W. Hillhouse, and R. Agrawal, *Nano Lett.*, 2009, **9**, 3060–5.

36. M. G. Panthani, V. Akhavan, B. Goodfellow, J. P. Schmidtke, L. Dunn, A. Dodabalapur, P. F. Barbara, and B. A. Korgel, *J. Am. Chem. Soc.*, 2008, **130**, 16770–16777.

37. S. E. Habas, H. A. S. Platt, M. F. A. M. van Hest, and D. S. Ginley, *Chem. Rev.*, 2010, **110**, 6571–94.

38. C. Nobile, L. Carbone, A. Fiore, R. Cingolani, L. Manna, and R. Krahne, *J. Phys. Condens. Matter*, 2009, **21**, 264013.

39. A. Guerrero-Martínez, J. Pérez-Juste, E. Carbó-Argibay, G. Tardajos, and L. M. Liz-Marzán, *Angew. Chem. Int. Ed. Engl.*, 2009, **48**, 9484–8.

40. D. Baranov, A. Fiore, M. van Huis, C. Giannini, A. Falqui, U. Lafont, H. Zandbergen, M. Zanella, R. Cingolani, and L. Manna, *Nano Lett.*, 2010, **10**, 743–9.

41. M. Yarema, M. V Kovalenko, G. Hesser, D. V Talapin, and W. Heiss, *J. Am. Chem. Soc.*, 2010, **132**, 15158–9.

42. M. P. Pileni, *Acc. Chem. Res.*, 2008, **41**, 1799–809.

43. A. Singh and K. M. Ryan, *Part. Part. Syst. Charact.*, 2013, 624–629.

44. R. Mainz, A. Singh, S. Levcenko, M. Klaus, C. Genzel, K. M. Ryan, and T. Unold, *Nat. Commun.*, 2014, **5**, 1–10.

TOC:

(A) Droplet based assembly
(i) Low concentration
(ii) Rail-track assembly
(iii) Vertically assembly
(B) Assembly in a vial
Non-Solvent
Buffer Layer
Nanorods suspension
Slow crystalisation
Hexagonal supercrystals
(C) Electrophoretic deposition
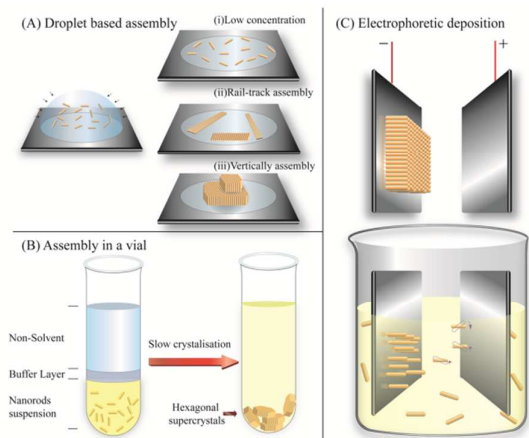
Abstract:

In this article we outline the assembly of binary, ternary and quaternary nanorods using three separate protocols. The rods are important photoabsorbers CdS, $CdSe_xS_{1-x}$, $CuIn_xGa_{1-x}S$, and Cu_2ZnSnS_4. In the droplet based assembly, we form either 1D rail-tracks or 2D discs of aligned rods depending on the net charge. In the vial based approach, we demonstrate crystallisation of rods into perfectly faceted hexagons. Finally we use electrophoretic deposition to assemble the charged rods directly at the substrate interface to obtain thin-films consisting of 50 or more nanorod layers obtained with complete orientational order.